

SAR-image derived soil moisture enhancement using GPR data

M. Nottebaere*, M.R. Ardekani*[†], S. Lambot[†] and X. Neyt*

*Signal and Image Centre, Royal Military Academy
30 Avenue de la Renaissance, 1000 Brussels, Belgium
martijn.nottebaere@elec.rma.ac.be

[†]Earth and Life Institute, Université catholique de Louvain
Croix du Sud 2 Box L7.05.02, 1348 Louvain-la-Neuve, Belgium

Abstract—Measuring the spatial distribution of soil moisture is important for agricultural, hydrological, meteorological and climatological research and applications. In this study, a new technique is developed to create soil moisture maps, based on the inversion of SAR measurements (RADARSAT-2, fine quad polarization) combined with GPR measurements. The Integral Equation Model is used to invert the SAR measurements, assuming a constant surface roughness and correlation length for the entire field, while the GPR data are inverted using a full wave inversion method. High resolution GPR measurements taken at different times under different land and weather conditions are used to generate a relative soil moisture landscape. We assume that these soil moisture difference patterns show little variation over time. By combining the inverted SAR data with a transformation of the soil moisture difference landscape, a high resolution soil moisture map is generated. The high resolution soil moisture maps show good agreement with the measured GPR soil moisture maps. The advantage of this technique is that once the relative soil moisture difference landscape is created, it allows the creation of new high resolution soil moisture maps later, by only taking a SAR image.

Index Terms—Inversion, GPR, SAR, soil moisture retrieval.

I. INTRODUCTION

Knowledge about the spatial distribution of soil moisture is important for agricultural, hydrological, meteorological and climatological research and applications. Techniques used for measuring the soil moisture include moisture probes, soil sampling, passive radiometry, ground penetrating radar (GPR) and synthetic aperture radar (SAR), each having their specific benefits and drawbacks [1]–[3]. The advantage of SAR is that with one satellite measurement, a large area can be sampled, but the drawback is the speckle. The benefit of GPR is that the spatial resolution can be much higher, but it is quite labor-intensive when the desired spatial resolution is very high.

The objective of this research is to find a technique that gets the benefits of both methods. As shown in [4], spatial soil moisture patterns do not show much temporal variation, meaning that the area of the field that is the wettest, will likely remain the wettest area of the field. Previous GPR data is used to characterize these soil moisture patterns. Knowledge of these patterns is used to improve the soil moisture estimation based on a single SAR image. To see if this method performs better than the classical multilook approach, results from both methods are compared to ground truth.

II. DATA

The field used for the measurement campaigns is a ~ 7 ha agricultural field located in the loess belt area in the central Belgium (Gembloux, Long. $4^{\circ}36'44''$ E, Lat. $50^{\circ}34'15''$ N), which is a test site of the Centre Wallon de Recherches Agronomiques (CRA). The elevation of the field ranges from 152.8 to 158.3 m a.s.l., which leads to a slope varying up to a maximum of 4.7 degrees across the field. The surface roughness of the field is about 1.2 cm.

The GPR data acquisition was done using a stepped-frequency continuous-wave (SFCW) GPR and a dGPS for positioning. The horn antenna used for these measurements (BBHA 9120 F, Schwarzbeck Mess-Elektronik) operates in the frequency range of 200-2000 MHz. This antenna is situated at a distance of ~ 50 cm above the soil surface. The used VNA was a ZVL system (Rohde & Schwarz, Munich, Germany) with a dynamic range of 70 dB, which was used with a step frequency of 10 MHz, and with the bandwidth set to the same value as the antenna bandwidth. All instruments were mounted on an all-terrain vehicle and the overall field was swept at an average velocity of 1 m/s following East-West oriented transects. The average distance between the different transects was about 3 m. The inversion of the data was done using the near-field full-wave inversion model of Lambot and André [5], to get the relative dielectric permittivity ϵ_r , and the model of Topp [6] was used to convert these values to volumetric soil moisture θ_v . For this inversion, only the frequencies below 1 GHz were used, since above this frequency, roughness effects influence the model [7].

The used SAR data was single-look-complex quad-polarization data from RADARSAT-2, which operates in C-band (5.4 GHz). The inversion was done using the integral equation model of Fung [8], [9], assuming that the surface roughness $k\sigma$ and the surface correlation kl are both equal to 1.2 cm. The assumption was made that multiple scattering is negligible, so the cross-polarization data was not taken into account for the inversion. The incidence angle contribution from the topography provided by the dGPS was also taken into account for the inversion.

In Table I, a summary of the measurement campaigns is given. During the first campaign the soil was partially frozen,

and during the second campaign it was dry and sunny.

TABLE I
SUMMARY OF THE MEASUREMENT CAMPAIGNS TAKEN FOR THIS RESEARCH.

Date	Field conditions	GPR datapoints
2013/03/27	Partially frozen	1794
2013/04/24	Sunny and very dry	4143

III. MODELS

A. General approach

As shown in [4], there is not much temporal variation in spatial soil moisture patterns. The first step of this method is to create a landscape $\delta(i)$ that characterizes these patterns, where i is the pixel coordinate. In a second step, a moisture model $\theta_m(i)$ is defined, that has this landscape and other parameters as input. By applying the Topp equation [6], we get the dielectric constant values $\varepsilon_m(i)$ at each pixel. With the model of Fung [8], [9], we can simulate the amplitude of the backscatter $\sigma_{VV,m}$ and $\sigma_{HH,m}$ at each pixel. In the final step, the values of the additional parameters of the moisture model $\theta_m(i)$ are estimated by fitting the backscatter values that result from the moisture model to the SAR backscatter. This can be done by minimizing the cost function:

$$J(m) = \langle (\sigma_{VV,m} - \sigma_{VV})^2 + (\sigma_{HH,m} - \sigma_{HH})^2 \rangle_i, \quad (1)$$

where σ_{HH} and σ_{VV} are the measured SAR backscatter amplitudes. The notation $\langle P \rangle_i$ is used for the mean value of $P(i)$ over all possible pixels i .

B. Landscape

Based on the GPR data from the first campaign, a moisture difference landscape is made

$$\delta(i) = \frac{\theta(i) - \langle \theta(i) \rangle_i}{\langle \theta(i) \rangle_i}, \quad (2)$$

where $\theta(i)$ is the moisture at point i , and $\langle \theta(i) \rangle_i$ is the average moisture of the entire field.

C. First landscape based model

The first moisture model $\theta_{m_1}(i)$ based on this landscape is defined as:

$$\theta_{m_1}(i) = \alpha + \beta \delta(i), \quad (3)$$

where α and β are fitting parameters. Based on this model, the value of the dielectric constant $\varepsilon_{m_1}(i)$ at each pixel i can be calculated by inverting the Topp equation [6]. We get the values of the backscatter σ_{VV,m_1} and σ_{HH,m_1} by applying the model of Fung [8], [9] to these dielectric constant values. To determine the values of the parameters α_0 and α_1 , we minimize the cost function J given in (1). We find the optimal values for the parameters α and β by applying a Nelder-Mead simplex method [10] to minimize this cost function.

D. Second landscape based model

To make the second model, we define ε_G as the dielectric constant we get when inverting the moisture from the first campaign θ_{GPR} with the equation of Topp. In the next step we define $\sigma_{G,pp}$ as the backscatter for polarization pp computed with the model of Fung. We then define

$$\delta_{S,pp}(i) = \frac{\sigma_{G,pp}(i) - \langle \sigma_{pp} \rangle_i}{\langle \sigma_{pp} \rangle_i}, \quad (4)$$

where σ_{pp} is the measured SAR backscatter of the first campaign. Based on this indicator, we can define the simulated backscatter as

$$\sigma_{sim,pp}(i) = a_{pp} + b_{pp} \delta_{S,pp}(i), \quad (5)$$

where a_{pp} and b_{pp} are fitting parameters. To find the best values for these parameters, we minimize the cost function

$$J = \langle (\sigma_{VV,sim} - \sigma_{VV,t})^2 + (\sigma_{HH,sim} - \sigma_{HH,t})^2 \rangle_i, \quad (6)$$

to get the optimal values for a_{VV} , b_{VV} , a_{HH} and b_{HH} . Based on these values, we compute the backscatter in both polarizations. The dielectric value at each pixel is then computed as

$$\hat{\varepsilon} = \arg \min_{\varepsilon} ((\sigma_{VV,sim} - \sigma_{VV}(\varepsilon))^2 + (\sigma_{HH,sim} - \sigma_{HH}(\varepsilon))^2). \quad (7)$$

With the Topp equation, these dielectric values are then converted to moisture values $\theta_{m_2}(i)$.

E. Reference models

To evaluate the performance of these methods, the obtained results are compared with those obtained with the classical multilook approach [11]. We define $\theta_{m_7}(i)$ as the moisture values that are obtained when applying a multilook filter of 7×7 pixels to the SAR data, before inverting them with the model of Fung. Similarly, $\theta_{m_9}(i)$ are defined as the moisture values that result from using a multilook filter of 9×9 pixels on the SAR data, before inverting them with the model of Fung.

F. Comparison to ground truth

To compare our model to these reference models, we define the ground truth moisture values $\theta_{GT}(i)$ for each pixel i as the average of the GPR moisture values measured in the last campaign in a radius of 8 m from the center of the pixel. Then we can define the error with respect to the ground truth for each model as

$$e_m(i) = \theta_m(i) - \theta_{GT}(i). \quad (8)$$

IV. RESULTS AND DISCUSSION

A. Reference models

The statistical parameters of the errors calculated with (8) are given in Table II. When comparing the moisture values from the reference models to the ground truth, we see that both reference models overestimate the moisture by 6.4% and 6.2% for m_7 and m_9 , respectively. To see if the moisture patterns of the field are well represented, we need to look at the standard

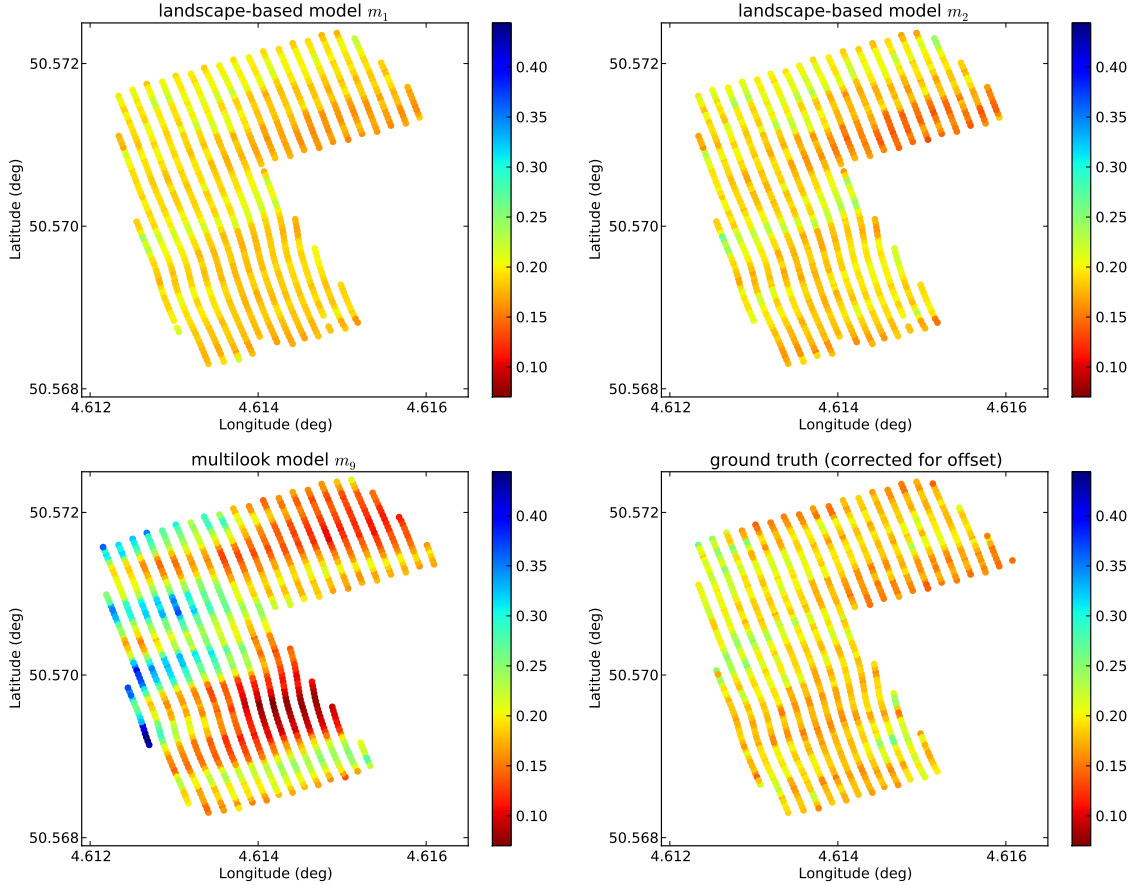


Fig. 1. Moisture values from the two discussed models m_1 and m_2 , the multilook model m_9 and the offset-corrected ground truth moisture, all in units of $\text{cm}^3.\text{cm}^{-3}$. An offset of 0.063 has been added to the ground truth moisture, to better visualize the difference in moisture patterns.

deviation. The standard deviation for m_7 is 7.0%, and for m_9 it is 5.8%, which is better. In figure 1, the moisture of the multilook model m_9 is shown, together with ground truth and the moisture values of the two discussed models.

TABLE II
STATISTICAL PARAMETERS OF THE COMPARISON BETWEEN THE MODEL MOISTURE VALUES AND THE GROUND TRUTH MOISTURE VALUES. ALL VALUES ARE IN UNITS OF $\text{CM}^3.\text{CM}^{-3}$.

model	e_m	
	mean	std
m_1	0.063	0.021
m_2	0.062	0.024
m_7	0.064	0.070
m_9	0.062	0.058

B. First landscape based model

To create the landscape for our first landscape based model θ_{m_1} , the GPR data from the first campaign is used to create

the indicator landscape with (2). Due to the spatial distribution of the points across the field, the values in this landscape are created with (9), by taking the average of this indicator in a radius of 8 m:

$$\delta(i) = \langle \delta(j) \rangle_{d(j,i) < 8m}, \quad (9)$$

where $d(j, i)$ is the distance between points i and j . In Fig. 2, this landscape is shown, for the spatial coordinates of the SAR pixels from the last campaign.

After determination of the coefficients α and β , the first landscape based model is

$$\theta_{m_1}(i) = 0.190 + 0.055\delta(i). \quad (10)$$

When comparing these moisture values with the ground truth, we find in Table II that similar to the reference models, the mean moisture of the field is overestimated by 6.3%. The standard deviation of the difference with the ground truth is 2.1%, which is much better than either of the reference models. This means that the spatial distribution of the soil moisture

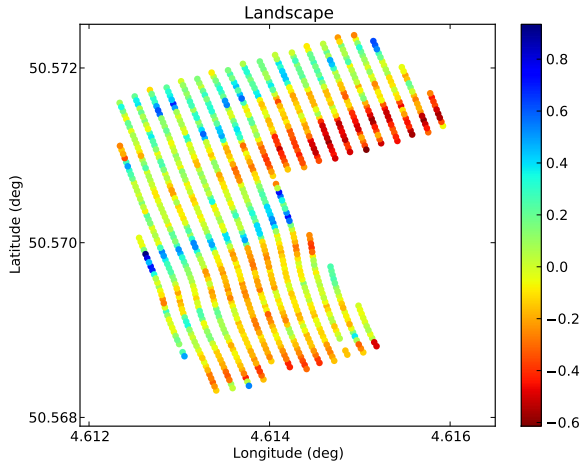


Fig. 2. Moisture landscape $\delta(i)$, as defined by (9), sampled at the location of the SAR pixels.

across the field is much better represented than in the reference models.

C. Second landscape based model

For the second landscape based model θ_{m_2} , after determining the coefficients a_{VV} , b_{VV} , a_{HH} , b_{HH} , the simulated backscatter is

$$\sigma_{Sim,VV}(i) = 0.083 + 0.013\delta_{S,VV}(i) \quad (11)$$

$$\sigma_{Sim,HH}(i) = 0.097 + 0.052\delta_{S,HH}(i) \quad (12)$$

From Table II, we see that the mean of the error is 6.2%, which is a similar overestimation as the other models. The standard deviation is 2.4%, indicating that this model fits the ground truth very well.

V. CONCLUSION

In this research a new method is presented to estimate the soil moisture based on the inversion of SAR data. Based on previous GPR measurements, a moisture landscape is generated which characterizes the relative soil moisture difference patterns. Two models to acquire the soil moisture based on this landscape and SAR data are analyzed and show good agreement when compared to ground truth data acquired with GPR. Both models give much better results than the soil moisture retrieved by the classical multilook approach for the inversion of SAR data.

ACKNOWLEDGMENT

This research was supported by the Belgian Science Policy Office in the framework of the SENSAR project of the Stereo II program.

REFERENCES

- [1] J. A. Huisman, S. S. Hubbard, J. D. Redman, and A. P. Annan, "Measuring soil water content with ground penetrating radar: A review," *Vadose Zone Journal*, vol. 2, pp. 476–491, 2003.
- [2] H. Vereecken, L. Weihermüller, F. Jonard, and C. Montzka, "Characterization of crop canopies and water stress related phenomena using microwave remote sensing methods: A review," *Vadose Zone Journal*, vol. 11, no. 2, 2012.
- [3] A. Ahmad, Y. Zhang, and S. Nichols, "Review and evaluation of remote sensing methods for soil-moisture estimation," *Journal of Photonics for Energy*, vol. 2, pp. 028 001–17, 2011.
- [4] J. Minet, N. E. C. Verhoest, S. Lambot, and M. Vanclooster, "Temporal stability of soil moisture patterns measured by proximal ground-penetrating radar," *Hydrology and Earth System Sciences Discussions*, vol. 10, no. 4, pp. 4063–4097, 2013.
- [5] S. Lambot and F. André, "Full-wave modeling of near-field radar data for planar layered media reconstruction," *IEEE Transactions on Geoscience and Remote Sensing*, vol. 52, no. 1, pp. 1–9.
- [6] G. Topp, J. L. Davis, and A. P. Annan, "Electromagnetic determination of soil water content: Measurements in coaxial transmission lines," *Water Resources Research*, vol. 16, pp. 574–582, 1980.
- [7] S. Lambot, M. Antoine, M. Vanclooster, and E. C. Slob, "Effect of soil roughness on the inversion of off-ground monostatic GPR signal for noninvasive quantification of soil properties," *Water Resources Research*, vol. 42, 2006.
- [8] A. K. Fung, Z. Li, and K. S. Chen, "Backscattering from a randomly rough dielectric surface," *IEEE Transactions on Geoscience and Remote Sensing*, vol. 30, pp. 356–369, Mar. 1992.
- [9] A. Fung, *Microwave Scattering and Emission Models and Their Applications*. Artech House, Incorporated, 1994.
- [10] J. A. Nelder and R. Mead, "A simplex method for function minimization," *The Computer Journal*, vol. 7, no. 4, pp. 308–313, 1965.
- [11] D. Thoma, M. Moran, R. Bryant, M. Rahman, C. H. Collins, T. Keefer, R. Noriega, I. Osman, S. Skrivin, M. Tischler, D. Bosch, P. Starks, and C. Peters-Lidard, "Appropriate scale of soil moisture retrieval from high resolution radar imagery for bare and minimally vegetated soils," *Remote Sensing of Environment*, vol. 112, no. 2, pp. 403 – 414, 2008.